Journal of Medicinal Chemistry

pubs.acs.org/jmc Article

Discovery of Anti-TNBC Agents Targeting PTP1B: Total Synthesis, Structure–Activity Relationship, *In Vitro* and *In Vivo* Investigations of Jamunones

Caijuan Hu, Guoxun Li, Yu Mu, Wenxi Wu, Bixuan Cao, Zixuan Wang, Hainan Yu, Peipei Guan, Li Han,* Liya Li,* and Xueshi Huang*

Cite This: *J. Med. Chem.* 2021, 64, 6008–6020 Read Online

ABSTRACT: Twenty-three natural jamunone analogues along with a series of jamunone-based derivatives were synthesized and evaluated for their inhibitory effects against breast cancer (BC) MDA-MB-231 and MCF-7 cells. The preliminary structure–activity relationship revealed that the length of aliphatic side chain and free phenolic hydroxyl group at the scaffold played a vital role in anti-BC activities and the methyl group on chromanone affected the selectivity of molecules against MDA-MB-231 and MCF-7 cells. Among them, jamunone M (JM) was screened as the most effective anti-triple-negative breast cancer (anti-TNBC) candidate with a high selectivity against BC cells over normal human cells. Mechanistic investigations indicated that JM could induce mitochondria-mediated apoptosis and cause G0/G1 phase arrest in BC cells. Furthermore, JM significantly restrained tumor growth in MDA-MB-231 xenograft mice without apparent toxicity. Interestingly, JM could downregulate phosphatidylinositide 3-kinase (PI3K)/Akt pathway by suppressing protein-tyrosine phosphatase 1B (PTP1B) expression. These findings revealed the potential of JM as an appealing therapeutic drug candidate for TNBC.

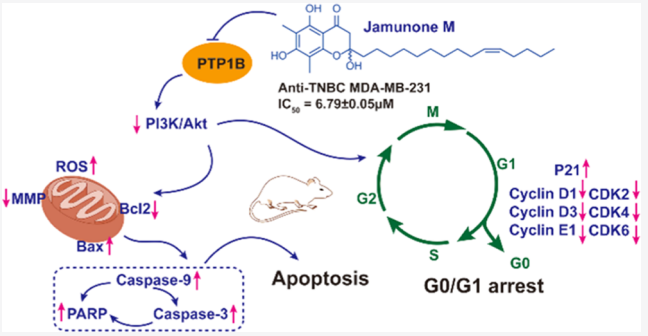

INTRODUCTION

Breast cancer (BC) has posed overwhelming threats to female health and quality of life with a high incidence and mortality.[1] As a complicated and heterogeneous malignant tumor, BC can be classified into distinct subtypes according to three immunophenotypes (ER: estrogen receptor; PR: progesterone receptor; HER2: human epidermal growth factor receptor 2).[2−4] Triple-negative breast cancer (TNBC) lacking the expression of ER, PR, and HER2 is regarded as an aggressive and intractable subtype of BC.[5,6] In fact, approximately 20% of invasive infection in breast cancer patients are caused by TNBC.[7,8] Although the current guidelines for BC treatment are mainly *via* surgery and chemotherapy,[9,10] there is still a significant challenge of clinical practices owing to lacking the effective target therapies and serious side effects.[11−14] The discovery of novel anti-BC agents to overcome or reduce multiple adverse effects remains an urgent priority.

Protein tyrosine phosphatases (PTPs) and protein tyrosine kinases (PTKs) are responsible for maintaining the balance of protein tyrosine phosphorylation levels and are involved in a host of cellular processes such as proliferation, differentiation, apoptosis, and survival.[15] As an important member of the PTP superfamily, PTP1B has been initially recognized as a negative regulator of insulin and leptin receptor signaling,[16] which has recently been verified to be overexpressed in TNBC and ER^+ BC.[17−19] A growing number of studies have confirmed that the frequent overexpression and amplification of PTP1B in BC cells are accountable for promoting proliferation, mitosis, and invasion.[20−23] Importantly, silencing PTP1B gene or down-regulating PTP1B protein level in BC cells can trigger cell cycle arrest and a series of apoptosis cascades.[24−26] PTP1B could be an effective target for the treatment of BC.

Recently, 16 plant-derived jamunone analogues (jamunones A–O and spiralisone C) with PTP1B inhibitory activity were reported by our research group.[27] In light of the important roles of PTP1B in cancer biology, we suspected that jamunones might have the potential of anti-BC effects. As expected, a preliminary bioassay screening discovered that these jamunones possessed antiproliferation activity against MDA-MB-231 (TNBC) and MCF-7 (ER^+ BC) at different thresholds. However, the lack of structural diversity and quantities of jamunones purified from natural source limited their further investigations on the

Received: January 18, 2021
Published: April 16, 2021

https://doi.org/10.1021/acs.jmedchem.1c00085
J. Med. Chem. 2021, 64, 6008–6020

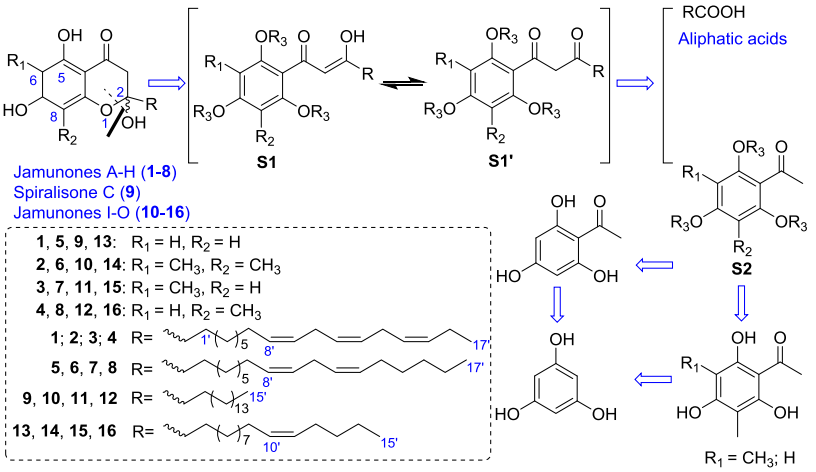

Figure 1. Structures and retrosynthetic analysis of jamunones **1**−**16**.

Scheme 1. Completion of Syntheses of Jamunones (1, 5, 9, 13) and JBs (1a−c, 5a−c, 9a−f, 13a−c)[a]

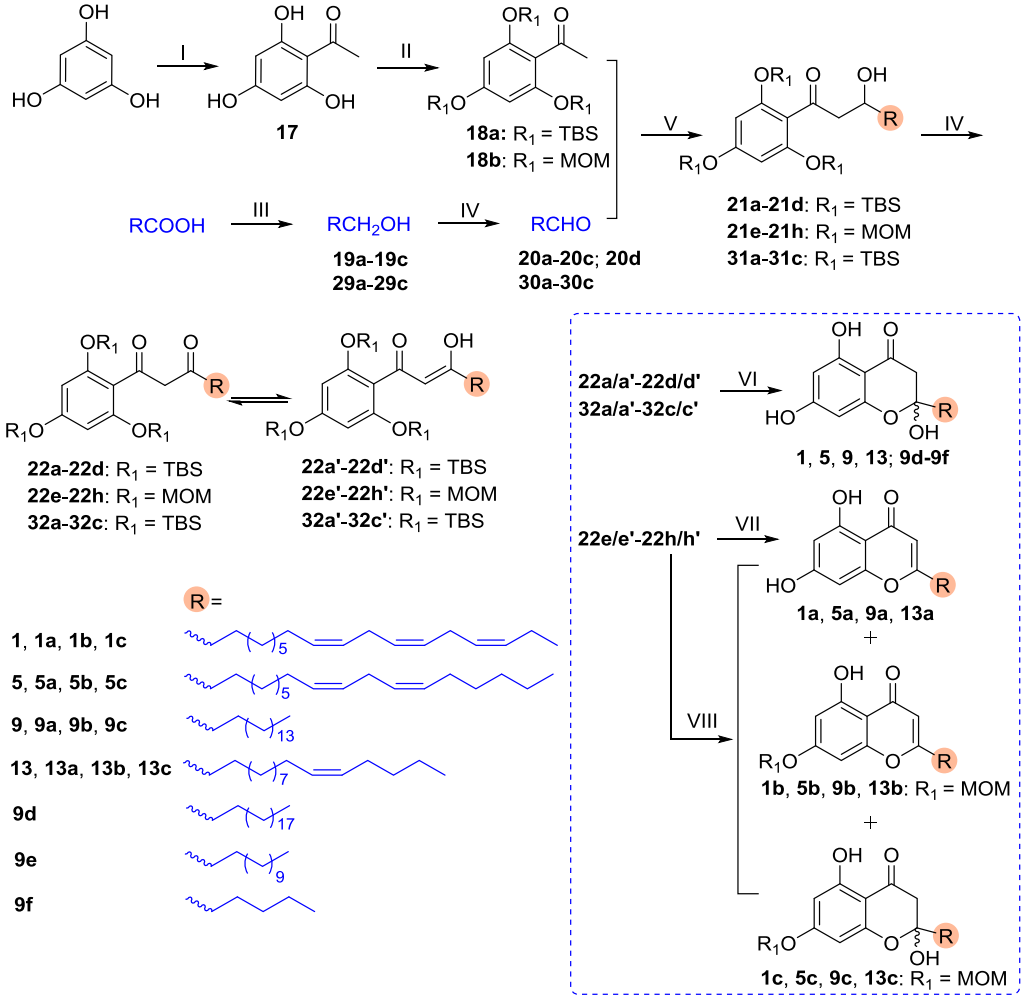

[a]Reagents and conditions: (I) Ac_2O, BF_3-OEt_2, AcOH, 100 °C, 6 h; (II) NaH, TBSCl/bromomethyl methyl ether (MOMBr), THF, 0 °C, 3 h; (III) lithium aluminum hydride (LAH), THF, 0 °C, 3 h; (IV) Dess−Martin periodinane (DMP), dichloromethane (DCM), 0 °C, 3 h; (V) LDA, THF, −78 °C, 12 h; (VI) TBAF, THF, room temperature (rt), 1 h; (VII) HCl/MeOH, 65 °C, 12 h; (VIII) TFA, DCM, 0 °C, 3 h.

structure−activity relationship (SAR) and the underlying mechanisms of anti-BC effect. To resolve the above queries, we had designed a novel and concise approach to synthesize 23 natural jamunone analogues, including jamunones A−O (**1**−**8** and **10**−**16**, respectively), spiralisone C (**9**), jambones E−G (**1a**, **3a**, **5a**),[28] samarones B−D (**6a**, **8a**, **2a**),[29] and 5,7-dihydroxy-2-pentadecylchromone (**9a**).[30] Meanwhile, a series of jamunone-based derivatives (JBs) were obtained using the same approach.

https://doi.org/10.1021/acs.jmedchem.1c00085
J. Med. Chem. 2021, 64, 6008−6020

Scheme 2. Completion of Syntheses of Jamunones (2−4, 6−8, 10−12, 14−16) and JBs (2a to 4a, 2b to 4b, 6a to 8a, 6b to 8b, 10a to 12a, 10b to 12b, 14a to 16a, 14b to 16b)[a]

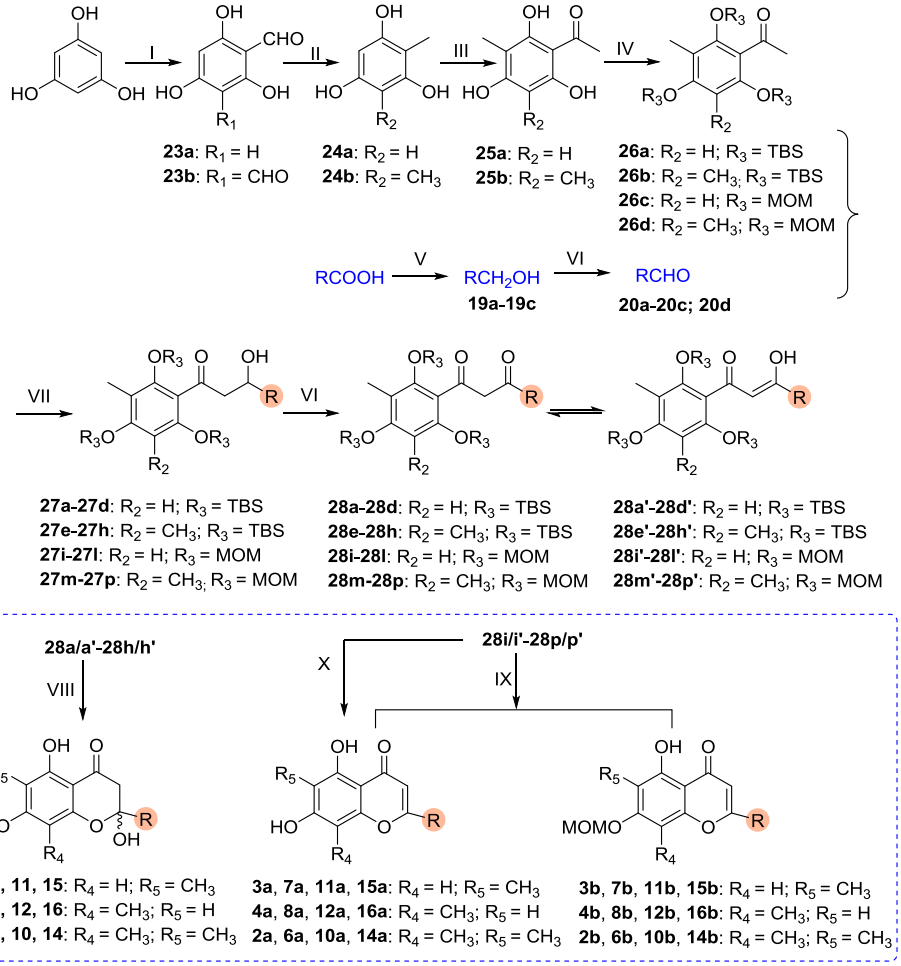

[a]Reagents and conditions: (I) $POCl_3$, *N*,*N*-dimethylformamide (DMF), 1,4-dioxane, 0 to 25 °C, 3 h; (II) $NaBH_3CN$, HCl, THF, 0 to 25 °C, 12 h; (III) Ac_2O, BF_3-OEt_2, AcOH, 100 °C, 3 h; (IV) NaH, TBSCl, THF, 0 °C, 2 h; (V) LAH, THF, 0 °C, 3 h; (VI) DMP, DCM, 0 °C, 3 h; (VII) LDA, THF, −78 °C, 12 h; (VIII) TBAF, THF, 0 °C, 1 h; (IX) TFA, DCM, 0 °C, 3 h; (X) HCl/MeOH, 65 °C, 12 h.

As a consequence, jamunone M (JM; **14**) was identified as the most efficacious drug lead for treating BC. Note that the highly selective activity of JM against BC cells was mainly due to restricting protein expression of PTP1B and downstream signaling pathway of phosphatidylinositide 3-kinase (PI3K)/Akt.

RESULTS AND DISCUSSION

Chemistry. The retrosynthetic analysis of jamunones **1**−**16** is illustrated in Figure 1. The disconnection of O1−C2 linkage leads to the formation of keto-enol tautomers **S1**/**S1′**. The pretarget molecules **S1**/**S1′** require the assembly from aliphatic acids and aromatic building block **S2**, which in turn originate from the acetylation and O-etherification of phloroglucinol (PG). With respect to methylated molecules, an extra methyl group is introduced onto the aromatic ring to eventually match the completion of their retrosynthetic approach.

Guided by the foregoing retrosynthetic strategy, our initial efforts were focused on the syntheses of jamunones **1**, **5**, **9**, and **13**. As outlined in Scheme 1, the synthetic protocol began with the preparation of the precursor **18a** from commercially available PG. PG was reacted with acetic anhydride to give the acetylation phenol **17** and subsequently treated with *tert*-butyldimethylsilyl chloride (TBSCl) to obtain *tert*-butyldimethylsilyl (TBS) ether **18a**. To introduce aliphatic side chains into the C-2 position of target molecules, aliphatic aldehydes **20a**−**d** were used in the following step. Aliphatic aldehydes **20a**−**c** were synthesized from fatty acids by a two-step sequence (reduction and oxidation reactions), and **20d** (*cis*-11-hexadecenal) was directly purchased from a commercial supplier. The aldol condensation of **18a** with **20a**−**d** furnished the key alcohols **21a**−**d** using lithium diisopropylamide (LDA) in tetrahydrofuran (THF) at −78 °C. These desired alcohols were further converted to inseparable keto−enol tautomers **22a**/**a′**−**d**/**d′** by Dess−Martin oxidation. Finally, the removal of TBS groups in the isomers **22a**/**a′**−**d**/**d′** using tetrabutylammonium fluoride (TBAF) proceeded smoothly to yield the desired jamunones **1**, **5**, **9**, and **13**. According to the similar synthetic strategy, nonadecyl, undecyl, and butyl groups were successfully grafted on the 5,7-dihydroxy chromanone scaffold to form JBs **9d**−**f**, respectively.

Following the synthetic methodologies of the isomers **22a**/**a′**−**d**/**d′**, the key precursors **22e**/**e′**−**h**/**h′** containing methoxymethyl (MOM) protecting groups were prepared. Afterward, the isomers **22e**/**e′**−**h**/**h′** degraded the MOM groups using trifluoroacetic acid (TFA) in one pot to give their structural

https://doi.org/10.1021/acs.jmedchem.1c00085
J. Med. Chem. 2021, 64, 6008−6020

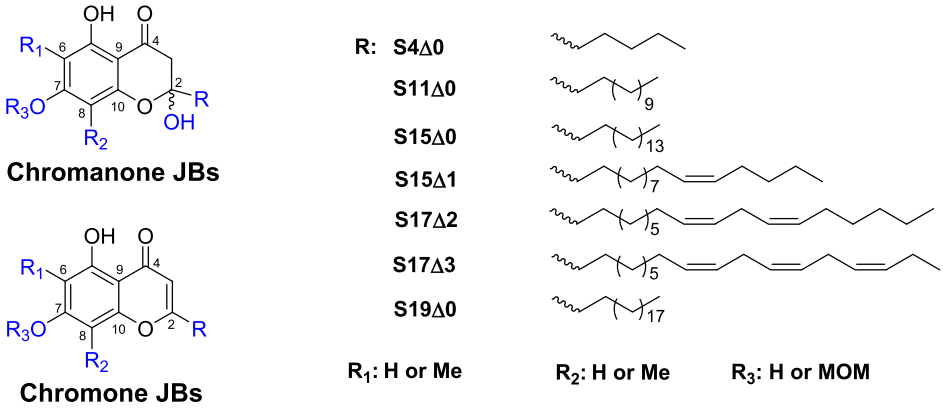

Figure 2. Primary structure−activity relationships of JBs.

analogues 7-OH-JBs (**1a**, **5a**, **9a**, **13a**) and 7-OMOM-JBs (**1b**, **5b**, **9b**, **13b**; **1c**, **5c**, **9c**, **13c**). Remarkably, these 7-OH-JBs (**1a**, **5a**, **9a**, **13a**) could be generated in a high yield under the HCl-catalyzed condition (Scheme 1).

Adhering to the similar logic to Scheme 1, the total syntheses of methylated jamunones (**2**−**4**, **6**−**8**, **10**−**12**, **14**−**16**), 7-OH-methylated JBs (**2a** to **4a**, **6a** to **8a**, **10a** to **12a**, **14a** to **16a**) and 7-OMOM-methylated JBs (**2b** to **4b**, **6b** to **8b**, **10b** to **12b**, **14b** to **16b**) were prospectively performed through using methylated PG instead of PG (Scheme 2). To implant a methyl group into PG skeleton, the starting material PG needed to undergo Vilsmeier−Haack formylation[31,32] and subsequent reduction with sodium cyanoborohydride[33] to provide the methylated intermediates (**24a**, **24b**), which allowed for the preparation of all associated intermediates.

Anti-BC Activity and Structure−Activity Relationships Studies of JBs. To investigate the inhibitory effects of synthesized JBs on TNBC MDA-MB 231 and ER$^+$ BC MCF-7 cells, an 3-(4,5-dimethylthiazol-2-yl)-3,5-phenytetrazoliumromide (MTT) assay was carried out. The half-maximal inhibitory concentration (IC_{50}) values of test compounds against BC cells are listed in Table S1. To analyze and characterize their anti-BC efficacy, a cluster dendrogram (Figure S1) was established in terms of their structural features and IC_{50} values. Taking their inhibitory effect and sensitivity against two BC cells as a standard, they were generally divided into four different clusters: cluster I, cluster II, cluster III, and cluster IV. Apparently, there was an overall trend for the anti-BC potency of JBs as follows: cluster II > cluster I > cluster IV ≈ cluster III.

Concretely, the JBs in cluster II had a diversity of chemical structures and preferable antiproliferative activity against MDA-MB-231 (IC_{50} = 6.79−38.73 μM) and MCF-7 (IC_{50} = 17.47−44.18 μM), which made cluster II play a predominant role in all of the clusters. By contrast, the JBs of cluster I possessed poor inhibitory effects on both MDA-MB-231 (IC_{50} = 42.77−54.31 μM) and MCF-7 cells (IC_{50} = 43.18−61.61 μM). Although the JBs in cluster IV were nearly noncytotoxic to ER$^+$ BC cell line MCF-7 (IC_{50} > 84.14 μM), they exhibited different susceptibility profiles against TNBC cell line (MDA-MB-231 IC_{50} = 16.09−65.95 μM), most notably jamunone I (**10**, MDA-MB-231: IC_{50} = 16.09 μM; MCF-7: IC_{50} > 100 μM). Different from other clusters, the JBs in cluster III were turned out to show extremely weak or no resistance to both BC cells (MDA-MB-231: IC_{50} > 87.02 μM; MCF-7: IC_{50} > 67.26 μM).

In accordance with the different potencies and sensitivities of JBs against MDA-MB-231 and MCF-7 cells, the cluster II could be further classified into four subclusters. Only jamunone L (**13**) distributing in subcluster 1 was more active against MCF-7 (IC_{50} = 18.73 μM) cell than MDA-MB-231 cell (IC_{50} = 33.93 μM). Furthermore, the inhibitory activity of JBs in subcluster 2 against TNBC cell (IC_{50} = 25.39−38.73 μM) was moderate and almost equivalent to their anti-ER$^+$ BC capacity (IC_{50} = 29.80−39.81 μM). Compared with other subclusters, the JBs in subclusters 3 and 4 had greater sensitiveness to MDA-MB-231 cell than MCF-7 cell. Impressively, jamunone M (**14**) in subcluster 3 displayed the highest sensitivity to MDA-MB-231 cell in synthesized JBs.

The chromanone-JBs (**1**, **5**, **9**, **13**) and chromone JBs (**1a**, **5a**, **9a**, **13a**) were randomly distributed in the different subclusters of cluster II. This phenomenon indicated that the fundamental structural units of chromanone and chromone played equally important roles in the pharmacophore of JBs, which encouraged us to further investigate the anti-BC SAR of JBs based on both structural scaffolds. To explore the effects of alkyl side chain on anti-BC potency, we constructed the derivatives **9d**−**f**. As shown in Figure S1, they were individually scattered in cluster I (**9e**) and cluster III (**9d**, **9f**), the inhibition effects of which on BC

https://doi.org/10.1021/acs.jmedchem.1c00085
J. Med. Chem. 2021, 64, 6008−6020

cells dramatically decreased or disappeared comparing to spiralisone C (**9**). It was deduced that extending/shortening the length of alkyl side chain at the C-2 site was unfavorable for promoting the antiproliferative activity (**9d**−**f** *vs* **9**). The number of carbon atoms of aliphatic chain ranging from 11 to 19 benefitted the inhibitory efficacy (**9** *vs* **9d**, **9e**). After that, the OMOM group was introduced onto the C-7 position to discuss the effect of the hydroxyl group on the activity. Among them, a majority of the 7-OMOM analogues (**5b** to **16b**, **2b**, **5c**, **9c**, and **13c**) were basically disseminated in clusters I, III, and IV, which indicated that the introduction of the OMOM moiety led to a sharp drop or loss of activity. From this, a hydrogen-bond donor group at the C-7 site was enormously favorable for improving the inhibitory potency.

To investigate the effect of methyl substitution on the anti-BC efficiency, a variety of methyl-substituted JBs were synthesized. As shown in Figure S1, they were scattered in different clusters with a rather distant phylogenetic relationship. The results indicated that the methyl substitution greatly affected the susceptibility against MDA-MB-231 and MCF-7 cells. Furthermore, most of methyl-substituted JBs were classified into those clusters with higher selectivity to MDA-MB-231 than MCF-7 cells (II-subclusters 3 and 4, and cluster IV). Note that the variation of alkyl side chain also influenced the activity of 6,8-dimethylated chromanone or chromone JBs. The substitution of an alkyl side chain of 15 carbon atoms (S15 alkyl chain) was beneficial for improving inhibitory effect against MDA-MB-231 cells in 6,8-dimethyl-chromanones (**10**, **14** *vs* **2**, **6**). However, S17 alkyl substitution was suitable for increasing the activity against MDA-MB-231 cell in 6,8-dimethyl-chromones (**2a**, **6a** *vs* **10a**, **14a**). Again, the degree of unsaturation of alkyl chain could impact the anti-BC property of JBs. For instance, jamunone I (**10**) with a saturated S15 alkyl substituent presented a higher selectivity for MDA-MB-231 over MCF-7 cells than that of JM (**14**) with an unsaturated S15 alkyl chain. However, JM showed stronger cytotoxicity against BC cells than jamunone I. To summarize, the primary SAR information is illustrated in Figure 2.

Cytotoxic Activity and Selectivity Index of JM. On the basis of the aforementioned analysis, JM exerted an optimal inhibitory effect on the proliferation of MDA-MB-231 (IC_{50}: 6.79 μM) and MCF-7 (IC_{50}: 17.47 μM) cell lines. To estimate the selective index (SI) of JM between cancer and normal cells,[34] the cytotoxicities of JM against a panel of different cancer cells and two normal human cells (HEK293T and human umbilical vein endothelial cell (HUVEC)) were assayed (listed in Table S2). As described in Figure 3A, the inhibitory activities of JM against BC cells were markedly superior to those of other cancer cells. Simultaneously, JM displayed satisfying selectivity to BC cells (SI: 2.08−6.78), especially the TNBC cells, MDA-MB-231 (SI 293T/TNBC: 5.35; HUVEC/TNBC: 6.78). Remarkably, the SI values of JM were about 2−7 times of doxorubicin (DOX) (Figure 3B). These data demonstrated that JM could be a potential candidate drug for targeting BC, especially TNBC.

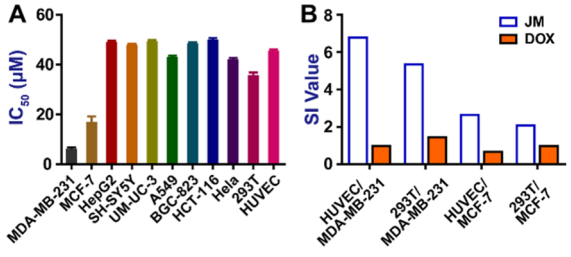

Figure 3. Representative bar graph illustrating the IC_{50} and SI values. (A) IC_{50} values of JM across a panel of cancer cell lines and two normal cell lines. (B) The SI values of JM and DOX (the ratio of IC_{50} value of normal cells to BC cells).

In view of the above observations, two questions were easily raised. (1) Did JM induce cell death *via* inhibiting the cell cycle or stimulating the apoptosis? (2) Among all of analogues, why did JM specifically target to TNBC cells?

***In Vitro* Antiproliferative Activities of JM.** To reveal the inherent mechanisms, we initially determined the effects of JM on the growth of two BC cells by MTT assay. As shown in Figure S2, JM suppressed the proliferation of BC cells in a time− and concentration−response curve. However, JM did not affect the viability of MDA-MB-231 and MCF-7 cells at concentrations of 5.0−0.56 and 15.0−1.67 μM, respectively, in 24 h. Therefore, these dosages of JM were selected for the following experiments.

JM Induced Mitochondrial Apoptosis in BC Cells. To further validate these observations, we next determined if JM had the ability to induce the apoptosis of BC cells. By Hoechst 33342 staining, JM-treated cells exhibited the typical features of apoptosis with chromatin shrinkage, membrane blebbing, and the formation of apoptotic bodies (Figure S3A,B). In addition, the flow cytometric analysis based on fluorescein isothiocyanate (FITC)-Annexin V/propidium iodide (PI) double staining showed that the total percentages of apoptotic cells (early and late apoptosis) in control groups were 3.5% (MDA-MB-231 cell) and 4.4% (MCF-7 cell), while the apoptosis ratios in JM-treated groups increased to 11.8 and 13.6%, respectively (Figure 4). Both assays implied that JM could trigger BC cell death through an apoptotic pathway.

The dysfunction of mitochondria has been reported to be responsible for apoptosis.[35,36] During the course of mitochondrial apoptosis, the intracellular reactive oxygen species (ROS) is highly induced.[37,38] The increasing levels of ROS can overoxidize cardiolipin in mitochondrial inner membrane, which promotes the decline of electron transfer chain function, leading to the variation of mitochondrial membrane potential (MMP) and cell apoptosis.[39]

To this end, we continued to inspect the production of ROS and levels of MMP in JM-treated BC cells. As shown in Figure S4A,B, the intensity of green fluorescence was notably enhanced in JM-treated BC cells compared to that of controls. Similarly, the results of flow cytometry exhibited the accumulation of ROS in JM-treatment BC cells (Figure S4C−F). Moreover, the MMP ($\Delta\Psi_m$) was monitored by the fluorescent probe JC-1. As described in Figure 5A, the intensity of green fluorescence was significantly increased and the intensity of red fluorescence was decreased in JM-treated BC cells. The results of flow cytometry disclosed a serious reduction of the ratio of red and green fluorescence in JM-treated groups (Figure 5B). In the meantime, the MMP levels in MDA-MB-231 and MCF-7 cells drastically dropped to 62.2 and 68.7%, respectively, in JM-treated cells (Figure 5C,D). These observations indicated the involvement of mitochondrial apoptosis in JM-treated cells.

Effect of JM on Apoptosis-Related Proteins. The mitochondria-dependent apoptotic pathway, also known as the intrinsic pathway, is primarily modulated by Bcl-2 family proteins.[40] An elevated ratio of pro-apoptotic protein Bax and anti-apoptotic Bcl-2 can strengthen the permeability of mitochondrial membrane and facilitate the release of apoptosis-inducing factors, leading to the activation of

https://doi.org/10.1021/acs.jmedchem.1c00085
J. Med. Chem. 2021, 64, 6008−6020

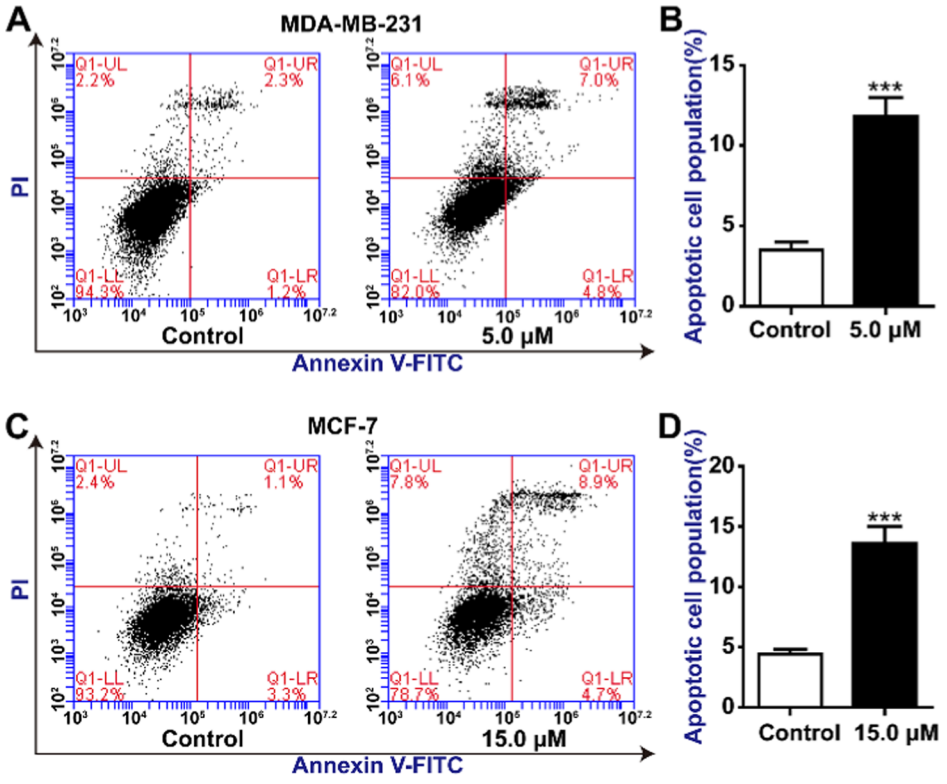

Figure 4. JM-induced BC cell apoptosis. (A, C) Apoptotic BC cells were analyzed with Annexin V-FITC/PI double staining in JM-treated BC cells. (B, D) Quantitative analysis of apoptosis rates by flow cytometry. ***$p < 0.001$ *vs* control.

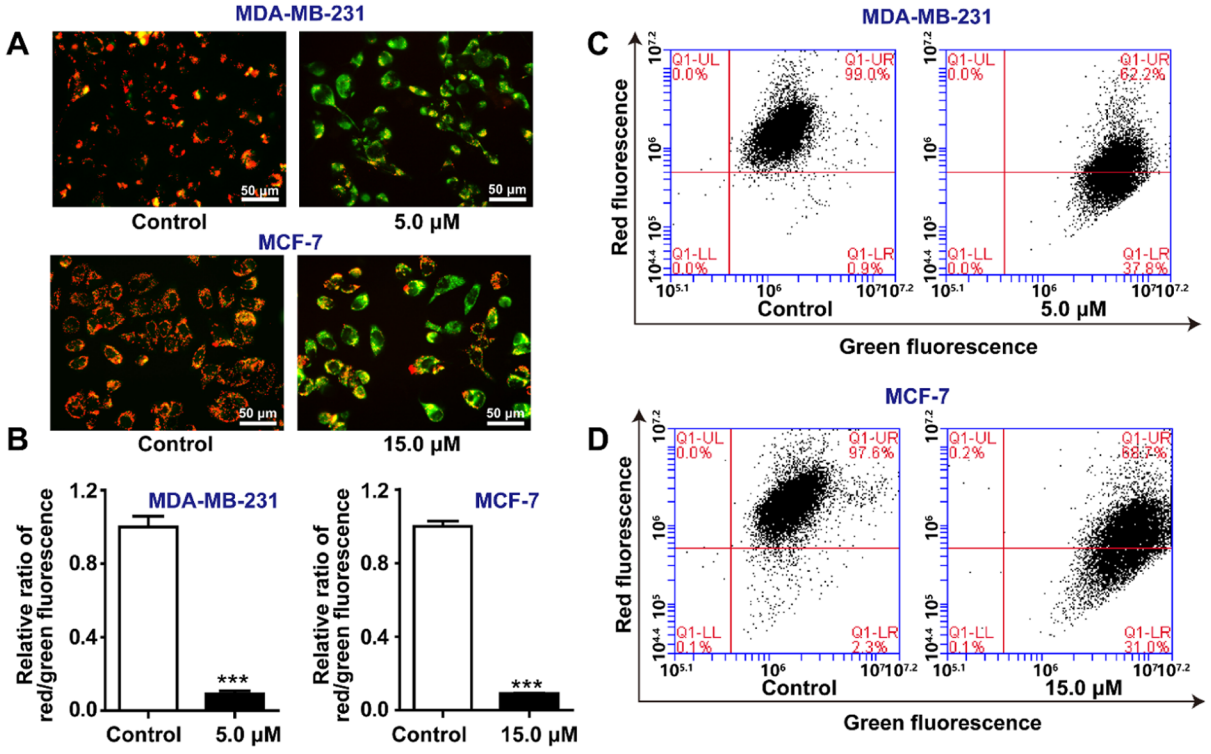

Figure 5. Effect of JM on MMP. (A) Fluorescence distribution in JM-treated BC cells for 24 h was observed under a fluorescence microscope. (B) Quantitative analysis of the mitochondrial membrane potential of BC cells. ***$p < 0.001$ *vs* control. (C, D) Changes of MMP level in BC cells were detected by flow cytometry analysis.

caspases.[41] As we know, caspase-9 and caspase-3 are critical for the cascade of apoptosis.[42] Caspase-9 has the ability to activate caspase-3, which results in cleaving diverse protein substrates (*e.g.*, poly(ADP-ribose) polymerase (PARP)) and participating in DNA fragmentation and reparation.[43] To further elucidate the mechanism of JM on apoptosis, the protein expression of

https://doi.org/10.1021/acs.jmedchem.1c00085
J. Med. Chem. 2021, 64, 6008−6020

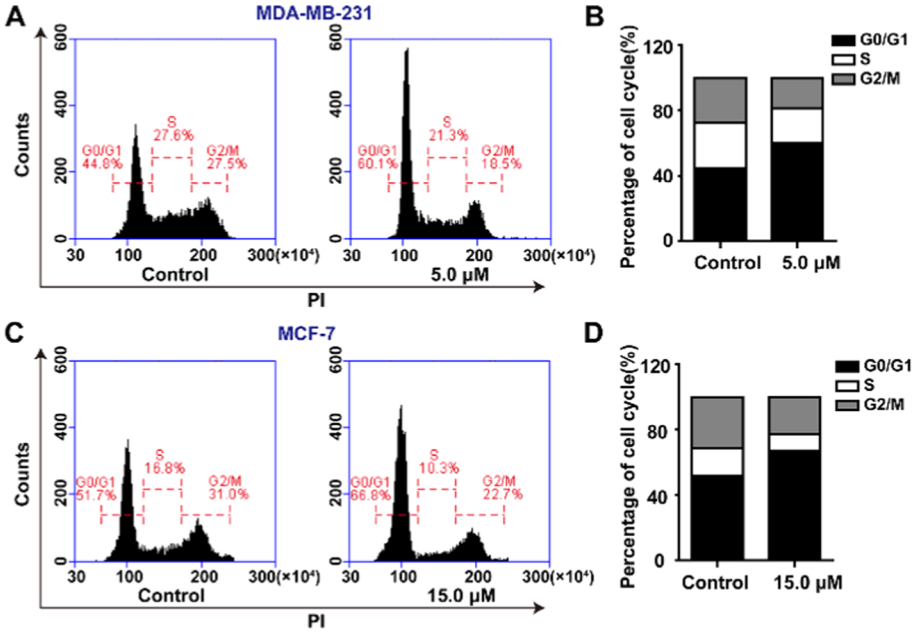

Figure 6. JM-caused G0/G1 phase arrest of BC cells. (A, C) Cell cycle distribution was analyzed by flow cytometry in BC cells treated with or without JM. (B, D) Statistical analysis of the cell cycle distribution of BC cells.

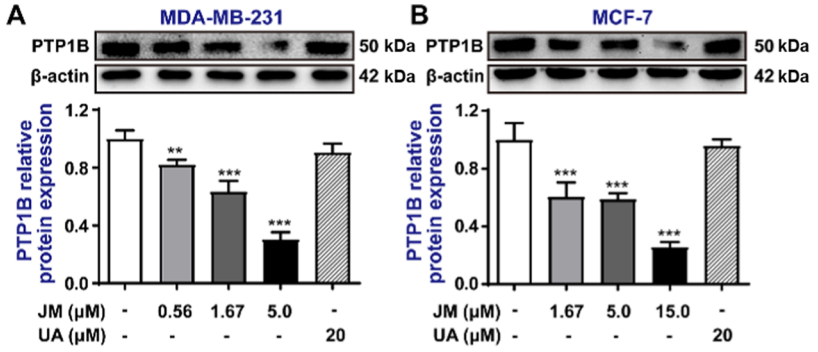

Figure 7. Effect of JM and UA on the expression of PTP1B protein. (A, B) Analysis of expression levels and relative quantities of PTP1B protein in BC cells determined by western blotting. $^{**}p < 0.01$ and $^{***}p < 0.001$ *vs* control.

caspases was examined by western blotting assay. As shown in Figure S5A−D, JM significantly increased the protein expression of Bax, and the production of cleaved caspase-9 and caspase-3 as well as decreased the level of Bcl-2 in a dose-dependent manner. Again, the cleaved protein level of poly(ADP-ribose) polymerase (PARP) was remarkably upregulated. On the basis of these observations, JM was found to induce cell death *via* the mitochondrial-dependent apoptotic pathway.

JM-Caused BC Cell G0/G1 Phase Arrest. The disorder of cell cycle will result in the occurrence and development of tumor.[44] Currently, multiple regulators of cell cycle are used as the targets of cancer therapy.[45] For these reasons, flow cytometry was carried out to determine the effects of JM on BC cells cycle. As depicted in Figure 6A−D, a large amount of cell population accumulated in the G0/G1 phase after treatment with JM for 24 h. The percentage of MDA-MB-231 cell in the phase of G0/G1 increased from 45.2% (control group) to 62.4% (JM-treated group). A similar result was obtained in MCF-7 cell with an increase from 51.7 to 66.8% after treatment with JM. These results revealed that JM could block BC cells in the phase of G1/G0.

Effect of JM on Cell Cycle-Related Proteins. For regulating cell cycle, cyclins, cyclin-dependent kinases (CDK) and CDK inhibitors (CKIs) play an important role.[46] The expression of D-type cyclin (cyclin D) occurs in the early phase of cell cycle, which combines CDK4 and CDK6 to generate a ternary complex, leading to initiation of the activities of CDK4 and CDK6.[47,48] In the late G1 stage, the complex of cyclin E and CDK2 will be formed to induce phase transition between G1 and S.[49] Besides, CKI p21 has the ability to negatively regulate the process of cell cycle by interacting with the cyclin E and CDK2.[50] In combination with these previous studies, western blots were performed to detect the expression of related regulators in JM-treated BC cells. As shown in Figure S6A,C, the protein expressions of cyclin D1, cyclin D3, cyclin E1, CDK2, CDK4, and CDK6 were downregulated in JM-treated groups, whereas the expression level of p21 was upregulated in a dose-dependent manner. These results verified our hypothesis that JM could effectively arrest cell cycle of BC cells at the G0/G1 phase *via* reducing the protein expression of cyclins and CDKs and enhancing the protein expression of p21 (Figure S6B,D).

JM Decreased PTP1B Expression Level in BC Cells. Until now, the effects of JM on suppressing the BC cells had

https://doi.org/10.1021/acs.jmedchem.1c00085
J. Med. Chem. 2021, 64, 6008−6020

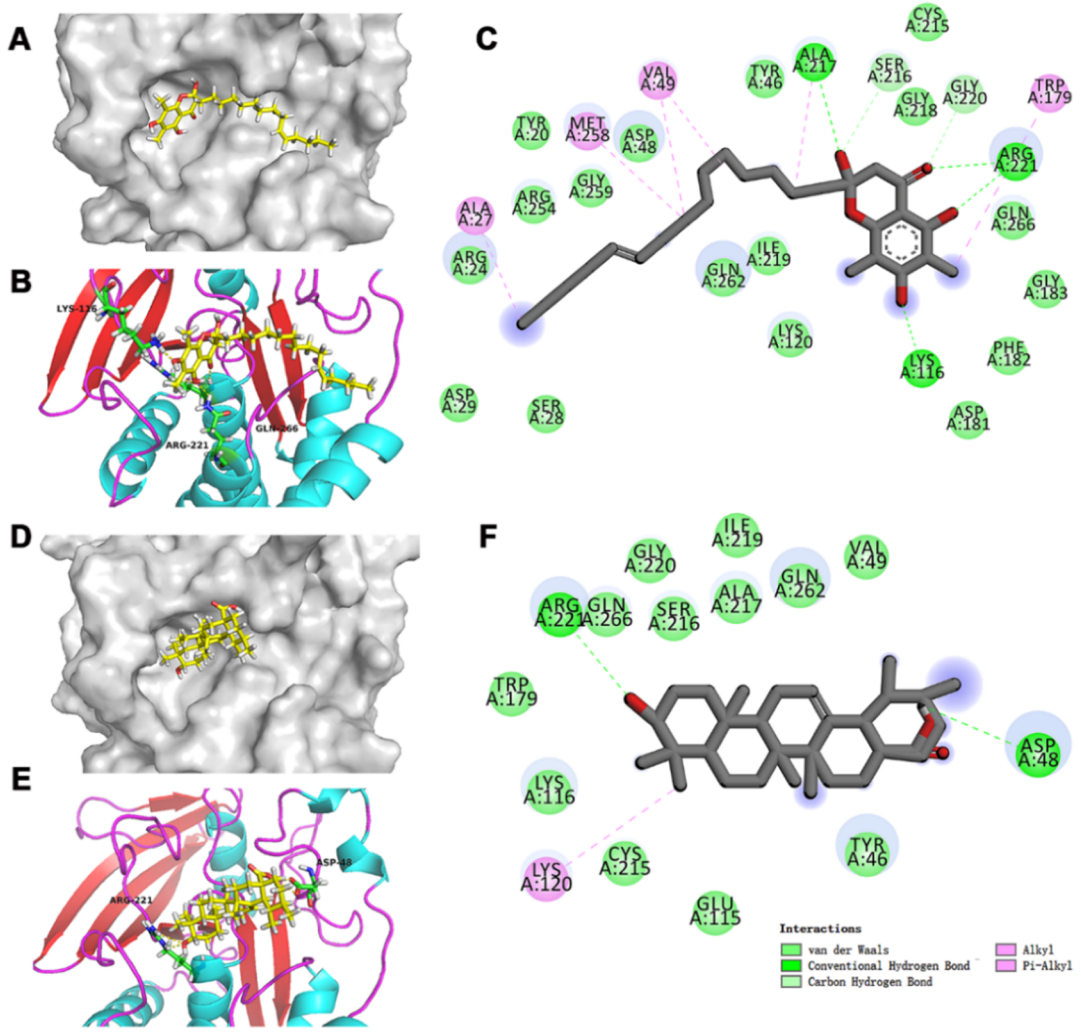

Figure 8. Binding mode of JM (A–C) and UA (D–F) to the active site of PTP1B. (A, D) Surface views of UA and JM with PTP1B. (B, E) Hydrogen-bond interactions of UA and JM with key amino acid residues. (C, F) Detailed interactions of UA and JM with key residues.

been found based on the above results. Nevertheless, it was still unclear that JM had a high selectivity toward TNBC cells relative to other jamunone-related analogues. Previously, our research had discovered that all of the tested jamunones had displayed a satisfying enzymatic inhibitory capacity of PTP1B,[27] which were superior to that of ursolic acid (UA, a positive control), especially jamunone A (**1**, IC_{50}: 0.45 μM) and jamunone E (**5**, IC_{50}: 0.42 μM). Although the enzyme-inhibiting activity of JM (IC_{50}: 1.80 μM) was lower than jamunones A and E, its activity of anti-BC was more efficacious than that of jamunones A and E. In consideration of these observations, the question was easily raised whether JM disturbed the expression of PTP1B in BC cells. For this purpose, the protein expression of PTP1B was determined by the western blotting assay in JM- or UA-treated BC cells. As expected, the protein level of PTP1B was significantly downregulated with increasing concentration of JM (Figure 7A,B). In contrast, UA had no effect on the expression of PTP1B. Hence, JM could exert anti-BC effects by specifically inhibiting the enzymatic activity and protein expression of PTP1B.

Molecular Docking. To further validate the targeting specificity of JM and visualize its potential binding mode, the docking studies were performed based on the crystal structure of human PTP1B (PDB code: 1NNY). As shown in Figure 8A,D, although JM showed the similar binding cavity in p-loop domain to UA, the chromanone core of JM was posed into the deeper bottom of active site than UA. Compared with UA, JM could establish the conventional hydrogen bonds not only with Arg221 through 5-hydroxyl and 4-carbonyl groups but also with Lys116 *via* 7-OH (Figure 8B,E). The generation of a hydrogen bond between Lys116 and 7-OH further highlighted the significant contribution of free OH group at the C-7 position in anti-BC activity, which was in line with the analysis of SAR. Note that the residue Ala217 from the P-loop oriented toward 2-OH and 2′-CH_2 groups of JM to generate hydrogen-bond and hydrophobic interactions, respectively (Figure 8C,F). Moreover, the alkyl–π interaction occurred between the 6-Me group of JM and the aromatic ring of Trp179, which supported this inference of SAR that methyl substitution on chromanone skeleton influenced the selectivity of molecules toward BC cells. Intriguingly, the alkyl chain of JM could extend toward a side pocket to form a long and narrow hydrophobic channel by participating in the multiple hydrophobic interactions with residues Val49, Met258, and Ala27, which might endow JM with high potency and good specificity over PTP1B.[51] The results led us to assume that the length and flexibility of hydrophobic side chain had an important influence on the binding affinity of JM to PTP1B. Accordingly, the binding action of JM with PTP1B

https://doi.org/10.1021/acs.jmedchem.1c00085
J. Med. Chem. 2021, 64, 6008–6020

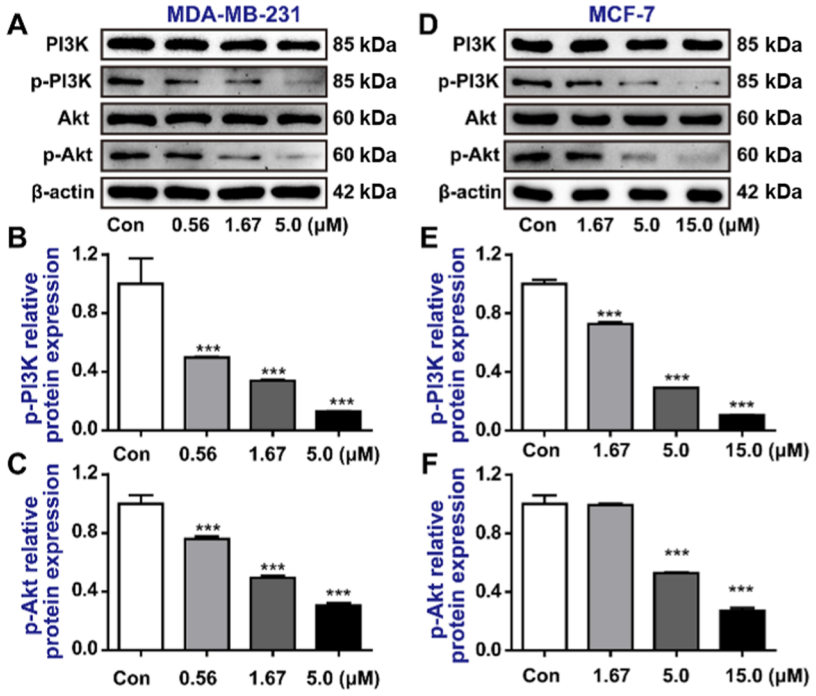

Figure 9. Effect of JM on PI3K/Akt signaling pathway. (A, D) Protein expressions of PI3K, p-PI3K, Akt, and p-Akt detected by western blotting in BC cells treated with various concentrations of JM. (B, C, E, F) Analysis of relative quantities of PI3K, p-PI3K, Akt, and p-Akt in BC cells. ***$p < 0.001$ *vs* Con.

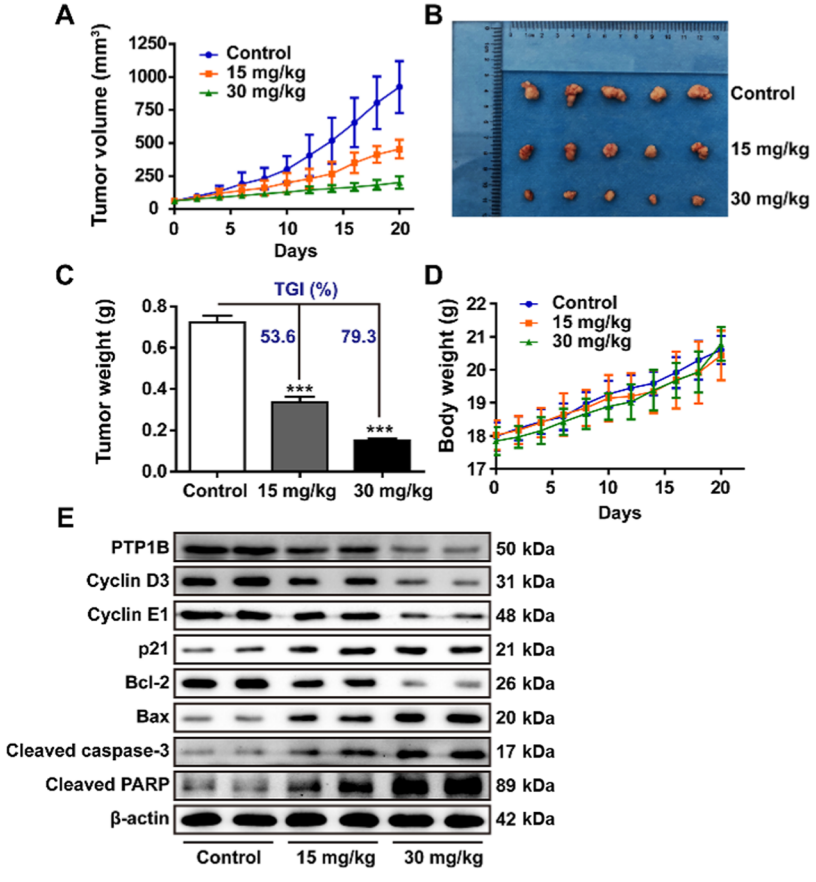

Figure 10. Antitumor activity of JM in mice bearing MDA-MB-231 xenograft. (A) Tumor volume of the mice was monitored during the experimental period. (B) Photographs of stripped tumors from each group. (C) Average tumor weights and inhibition rates measured after the mice were sacrificed. (D) Variation of mice body weight throughout the experiment. (E) Expression levels of PTP1B, Bcl-2, Bax, cleaved caspase-3, cleaved PARP, cyclin D3, cyclin E1, and p21 proteins in xenograft tumors analyzed by western blotting.

https://doi.org/10.1021/acs.jmedchem.1c00085
J. Med. Chem. 2021, 64, 6008−6020

could provide precious information for a future lead optimization.

JM Downregulated PI3K/Akt Signaling Pathway in BC Cells. The PI3K/Akt signaling pathway plays a central role in intracellular signal transduction, which participates in regulating various cell functions, including proliferation, survival, metastasis, metabolism, angiogenesis, *etc.*[52] More recently, the overexpression of oncogenic PTPs results in hyperactivating the PI3K pathway in some human cancers, leading to the promotion of tumor growth and development.[53] For these reasons, western blot analysis was carried out to check if the inhibitory effect of JM on BC cells was mediated by the PTP1B/PI3K/Akt pathway. The protein expression of PI3K p85 and Akt in JM-treated BC cells were not altered compared to that of the control group, but the phosphorylation levels of PI3K and Akt were apparently inhibited in a concentration-dependent manner (Figure 9A–F). Consequently, our data suggested that JM might block cell proliferation and induce cell apoptosis by targeting PTP1B and deactivating the PI3K/Akt pathway.

JM-Suppressed MDA-MB-231 Xenograft Growth *In Vivo*. Following the excellent selectivity of JM for TNBC *in vitro*, we established an MDA-MB-231 xenograft mouse model to evaluate the inhibitory efficacy of JM on TNBC *in vivo*. As depicted in Figure 10A,B, the growth rate and tumor size in mice were substantially retarded with increasing the dosage of JM. Compared with the control group, the inhibiting values of tumor growth inhibition (TGI, %T/C) at 15 and 30 mg/kg dosage of JM for 20 days were up to 53.6 and 79.3%, respectively (Figure 10C). Notably, there were no significant changes in body weights among the three groups, which demonstrated no severe toxicity of JM in mice (Figure 10D). Consistent with *in vitro* study, our *in vivo* study indicated that the expression levels of Bax, cleaved caspase-3, cleaved PARP, and p21 were dramatically upregulated, whereas cyclin D3, cyclin E1, and Bcl-2 expressions were downregulated in the JM-administered mice (Figure 10E). Moreover, the PTP1B protein expression of tumor tissue obviously decreased in JM-administered groups. As a result, JM could target PTP1B and restrain the growth of MDA-MB-231 tumor xenograft *via* inducing apoptosis and cell cycle arrest.

CONCLUSIONS

In summary, we elaborated the total synthesis of jamunones and deduced the primary SAR of anti-BC. The meaningful SARs can be drawn as follow: (i) hydroxyl group at the C-7 position is essential for activity; (ii) the length of alkyl side chain ranging from 11 to 19 carbon atoms is favorable for anti-BC activity; (iii) the 6,8-dimethyl substitution in chromanone or chromone scaffold benefits to improve the selectivity toward TNBC cell. JM was screened out as a highly selective candidate for treating TNBC. The in-depth biological investigations revealed distinct morphological changes, an excess ROS production, a downward $\Delta\Psi_m$, apoptotic induction, and cell cycle blockage at the G0/G1 phase in JM-treated BC cells. The anti-BC feature of JM was found to target PTP1B, which resulted in deactivating PI3K/Akt pathway. Subsequently, the docking profile indicated that the formation of multiple hydrogen bonds and hydrophobic tunnel ensured the stable fit of JM in the catalytic domain of PTP1B, further elucidating the targeting ability of JM and some significant SARs. More importantly, JM dramatically inhibited tumor growth in the MDA-MB-231 tumor xenografts without obvious toxicity. All in all, these findings identified JM as an attractive drug candidate for PTP1B-targeted TNBC therapy.

EXPERIMENTAL SECTION

General Methods. All of the reagents and solvents were purchased from commercial suppliers and used without further purification unless otherwise indicated. Reactions were cooled using a cryocooler or external cooling baths (−78 °C or ice water 0 °C). Heating was achieved using a silicone oil bath with heating controlled by an electronic contact thermometer. Reaction courses were monitored by thin-layer chromatography (TLC) on silica gel-precoated F254 Merck plates. Purification of reaction mixtures was performed by column chromatography using silica gel (100–200 mesh, 200–300 mesh, Qingdao Marine Chemical Ltd., Qingdao, China). All of the intermediates and target compounds were fully analyzed and characterized by ^{1}H and ^{13}C NMR spectra, high-resolution mass spectra (HRESI-MS), ultraviolet (UV) spectra, and infrared (IR) spectra before biological screening. The following abbreviations were used to designate the multiplicities: s = singlet, d = doublet, t = triplet, q = quartet, qn = quintet, m = multiplet, br = broad. All of the targeted compounds were analyzed by high-performance liquid chromatography (HPLC) with a UV–visible detector (2 μm, 50 mm × 2.0 mm, Agilent YMC-UltraHT Pro C18), eluted at 0.35 mL/min with MeOH/water + 5% MeCN + 0.1% formic acid (gradient: 85–95% in 25 min). The purities of compounds were confirmed as ≥95%.

Cell Culture and Cell Viability Assay. All of the cell lines used in our study (obtained from the Chinese Academy of Science, Shanghai, China) were cultured in Dulbecco's modified Eagle's medium (DMEM) supplemented with 10% fetal bovine serum (FBS), 1% L-glutamine, 100 units/mL penicillin, and 100 μg/mL streptomycin at 37 °C in a humidified 5% CO_2 atmosphere incubator (Thermo Fisher Scientific, Waltham, MA). The cytotoxicity and proliferation inhibition were quantified by the MTT assay. The results were represented as mean ± standard deviation (SD) from three independent experiments. The inhibition rate (%) = $[A_{570}$ (control) − A_{570} (compound)$]/A_{570}$ (control) × 100%. The IC_{50} values were calculated by a nonlinear regression analysis using SPSS 13.0 (SPSS, Inc., Chicago, IL).

Cluster Analysis Assay. Based on the Euclidean distance of the IC_{50} values of test compounds against BC cells, cluster analysis was performed to characterize their anti-BC potency and structural features using the "ggplot2" package in the program R 4.0.2 (R Core Team, 2020).

Hoechst 33342 Staining. Cells stained with Hoechst 33342 (Beyotime Biotechnology Co., Shanghai, China) were widely used to evaluate nuclear morphological changes. MDA-MB-231 and MCF-7 cells (6×10^4 cells/well) were seeded in 24-well plates and treated with different concentrations of JM (0 and 5.0 μM for MDA-MB-231; 0 and 15.0 μM for MCF-7) for 24 h. Subsequently, the cells were washed three times with phosphate-buffered saline (PBS) and stained with 1 mL suspension of Hoechst 33342 and PBS for 5 min in the dark at rt. The changes in nuclear morphology were evaluated and photographed by a fluorescence microscope (Leica, Wetzlar, HE, Germany).

Cell Apoptosis Assay. MDA-MB-231 and MCF-7 cells (3×10^5 cells/well) were seeded in six-well plates and exposed to compound JM (0 and 5.0 μM for MDA-MB-231; 0 and 15.0 μM for MCF-7) for 24 h. Afterward, the cells were collected, washed with cold PBS, and resuspended in 195 μL of binding buffer. Fluorescein isothiocyanate (FITC)-conjugated annexin-V reagent (1 μL) and PI (8 μL, BD, Franklin Lakes, NJ) were added to the samples and mixed gently. After 15 min incubation in the dark at room temperature, the samples were immediately run on an LSR-Fortessa flow cytometer and analyzed with the Annexin V-FITC/PI apoptosis method. Cytographs were performed using BD FACSDiva software (BD, Franklin Lakes, NJ). Each experiment was conducted three times.

Reactive Oxygen Species (ROS) Assay. The formation of intracellular ROS was assessed using a ROS Assay kit (Beyotime Biotechnology Co., Shanghai, China). MDA-MB-231 and MCF-7 cells (6×10^4 cells/well) were seeded in 24-well plates with 5.0 and 15.0 μM of M treatment for 24 h, respectively. After washing once with PBS, these cells were stained with 10 μM dichlorodihydrofluorescein diacetate (DCFH-DA) at 37 °C for 30 min in the dark, washed three times with serum-free medium, and then resuspended in serum-free

https://doi.org/10.1021/acs.jmedchem.1c00085
J. Med. Chem. 2021, 64, 6008–6020

medium. The alteration of fluorescence intensity was observed under a fluorescence microscope.

MDA-MB-231 and MCF-7 cells (3×10^5 cells/well) were seeded into six-well plates and treated with JM (0 and 5.0 μM for MDA-MB-231; 0 and 15.0 μM for MCF-7) for 24 h. The cells were washed once with PBS, incubated with 10 μM DCFH-DA at 37 °C for 30 min in the dark. Then, the cells were washed three times with serum-free medium, centrifuged (1000 rpm, 5 min), and collected. Finally, the cells were resuspended by the addition of 500 μL of PBS and loaded onto a flow cytometer.

Mitochondrial Membrane Potential (MMP) Assay. The mitochondrial membrane potential ($\Delta\Psi_m$) was measured with an MMP assay kit with JC-1 (Beyotime Biotechnology Co., Shanghai, China). MDA-MB-231 and MCF-7 cells (6×10^4 cells/well) were seeded in 24-well plates. After 24 h incubation, the cells were treated with JM (0 and 5.0 μM for MDA-MB-231; 0 and 15.0 μM for MCF-7) for another 24 h. The cells were washed once with PBS. After that, 0.4 mL of the cell culture solution and 0.4 mL of JC-1 staining working solution were successively added, thoroughly mixed, and incubated at 37 °C for 20 min in the dark. The cells were washed twice with JC-1 staining buffer (1×) and resuspended in fresh culture medium. Finally, mitochondrial membrane potential was evaluated qualitatively under a fluorescence microscope.

MDA-MB-231 and MCF-7 cells (3×10^5 cells/well) were incubated with different concentrations of JM (0 and 5.0 μM for MDA-MB-231; 0 and 15.0 μM for MCF-7) in six-well plates. After treatment with 24 h, 1 mL of the cell culture media and 1 mL of JC-1 staining working solution was added, mixed well, and incubated at 37 °C for 20 min. Later, the cells were centrifuged (1000 rpm, 5 min) and washed twice by 1× JC-1 staining buffer. The collected cells were resuspended in 500 μL of JC-1 staining buffer and immediately analyzed by a flow cytometer.

Cell Cycle Assay. MDA-MB-231 and MCF-7 cells (3×10^5 cells/well) were seeded in six-well plates and exposed to compound JM (0 and 5.0 μM for MDA-MB-231; 0 and 15.0 μM for MCF-7) for 24 h. The cells were then collected and fixed overnight in 75% ethanol at −20 °C. The next day, the cells were washed twice with cold PBS, gently resuspended in 500 μL of propidium iodide (PI) working fluid (Dingguo Changsheng Biotechnology Co. Ltd., Beijing, China), and incubated for 15 min in the dark at rt. Cell cycle analysis was performed using an LSR-Fortessa flow cytometer. The percentage of cells in each phase was analyzed using ModFit LT 4.1 software (Verity Software House, Topsham, ME). Each experiment was conducted three times.

***In Vivo* Xenograft Study.** A 150 μL MDA-MB-231 cell suspension (6×10^6 cells in PBS) was subcutaneously inoculated into the right back of 8-week-old female BALB/c nude mice (Changsheng Biotechnology Co., Ltd., Liaoning, China). When the average volume of the tumors reached about 60 mm^3, the mice were randomized into three groups (n = 5/group). The control group (vehicle) and two JM treatment groups (15, 30 mg/kg) were intraperitoneally injected every other day for 10 treatments. Tumor volume and body weight were recorded every other day after drug treatment. After 20 days, all mice were sacrificed and the tumors were harvested for further study. The tumor size was calculated by the equation: V (tumor volume, mm^3) = L (length, mm) × W^2 (width, mm) × 0.5. The tumor growth inhibition (TGI) ratio was calculated with the following formula: TGI = $(1 - TW_t/TW_c) \times 100\%$, where TW_t and TW_c represent average tumor weight of JM-treated and control groups on day 20, respectively. All animal procedures were conducted in accordance with the NIH Guidelines for the Care and Use of Laboratory Animals (Institute of Laboratory Animal Resources, 1996) and were approved by the Animal Care and Use Committee of Northeastern University (Shenyang, China, 2016.04).

Molecular Modeling Study. The available X-ray structure of PTP1B (PDB ID: 1NNY)[54] was downloaded from Protein Data Bank (http://www.rcsb.org/pdb). Docking study was conducted using Discovery Studio 3.5. The binding site was defined according to the reference ligand by a radius of 10.5 Å. The protein structure was processed by removing water molecules, adding hydrogen atoms, and applying Charmm forcefield. The ligands were prepared by adding hydrogen atoms and energy minimization. Gold score protocol was used as the score function, and the other parameters were set as default. The results were processed by PyMoL.[55]

Western Blotting Analysis. The *in vitro* effect of JM on protein expression was examined in MDA-MB-231 and MCF-7 cells. MDA-MB-231 and MCF-7 cells were seeded in six-well plates with a density of 3×10^5 cells/well and treated with various concentrations of JM (0, 0.56, 1.67, and 5.0 μM for MDA-MB-231; 0, 1.67, 5.0, and 15.0 μM for MCF-7) for 24 h. The treated cells were washed with cold PBS and lysed with radioimmunoprecipitation assay (RIPA) lysis buffer (Beyotime Biotechnology Co., Shanghai, China) containing 2% protease inhibitor cocktail and 1% phosphatase inhibitor cocktail (Promega, Madison, WI). In *in vivo* experiment, tumor tissue homogenate was lysed for western blotting. Protein concentration was determined by a bicinchoninic acid (BCA) protein assay kit (Beyotime Biotechnology Co., Shanghai, China). Equal quantities of protein were separated by 10 or 12% sodium dodecyl sulfate-polyacrylamide gel electrophoresis (SDS-PAGE), electroblotted to poly(vinylidene difluoride) (PVDF) membranes (Millipore, Billerica, MA), and blocked with 5% nonfat milk for 60 min at rt. The membranes were incubated with specific primary antibodies (diluted 1: 3000 in 1× Tris-buffered saline) overnight at 4 °C.

After washing three times with TBST, the membranes were probed with the corresponding secondary antibodies (diluted 1:10 000 in 5% nonfat milk) for 60 min at rt. Then, protein bands were detected with ECL select western blot detection reagent (Millipore, Billerica, MA) by chemiluminescence (Tanon 5500, Shanghai, China). Each protein band was normalized to the respective anti-β-actin band. The GIS Gel Image System (Tanon, Shanghai, China) was used for the quantitative grayscale analysis of the bands. Again, the primary antibodies for Bax, Bcl-2, caspase-3, caspase-9, PARP, cyclin D1, cyclin D3, cyclin E1, CDK2, CDK4, CDK6, p21, Akt, phospho-Akt, PI3K, phospho-PI3K, β-actin, and horse-radish peroxidase (HRP)-conjugated secondary antibodies were purchased from Cell Signaling Technology (Dancers, MA), apart from the primary antibodies for PTP1B (Absin Bioscience, Inc., Shanghai, China).

■ ASSOCIATED CONTENT

Supporting Information

The Supporting Information is available free of charge at https://pubs.acs.org/doi/10.1021/acs.jmedchem.1c00085.

Synthetic procedures, characterization data, and NMR spectra for all listed compounds; HPLC chromatogram of lead compounds; and some biological data (PDF)

Molecular formula strings (CSV)

Accession Codes

PDB code 1NNY was used for modeling docking in PTP1B of JM. The authors will release the atomic coordinates and experimental data upon article publication.

■ AUTHOR INFORMATION

Corresponding Authors

Li Han − *Institute of Microbial Pharmaceuticals, College of Life and Health Sciences, Northeastern University, Shenyang 110819, China*; Email: hanli@mail.neu.edu.cn

Liya Li − *Institute of Microbial Pharmaceuticals, College of Life and Health Sciences, Northeastern University, Shenyang 110819, China*; orcid.org/0000-0002-1894-9500; Email: lyli@mail.neu.edu.cn

Xueshi Huang − *Institute of Microbial Pharmaceuticals, College of Life and Health Sciences, Northeastern University, Shenyang 110819, China*; orcid.org/0000-0002-1561-8108; Email: huangxs@mail.neu.edu.cn

https://doi.org/10.1021/acs.jmedchem.1c00085
J. Med. Chem. 2021, 64, 6008−6020

Authors

Caijuan Hu − *Institute of Microbial Pharmaceuticals, College of Life and Health Sciences, Northeastern University, Shenyang 110819, China*

Guoxun Li − *Institute of Microbial Pharmaceuticals, College of Life and Health Sciences, Northeastern University, Shenyang 110819, China*

Yu Mu − *Institute of Microbial Pharmaceuticals, College of Life and Health Sciences, Northeastern University, Shenyang 110819, China*

Wenxi Wu − *Institute of Microbial Pharmaceuticals, College of Life and Health Sciences, Northeastern University, Shenyang 110819, China*

Bixuan Cao − *Institute of Microbial Pharmaceuticals, College of Life and Health Sciences, Northeastern University, Shenyang 110819, China*

Zixuan Wang − *Institute of Microbial Pharmaceuticals, College of Life and Health Sciences, Northeastern University, Shenyang 110819, China*

Hainan Yu − *Institute of Microbial Pharmaceuticals, College of Life and Health Sciences, Northeastern University, Shenyang 110819, China*

Peipei Guan − *Institute of Microbial Pharmaceuticals, College of Life and Health Sciences, Northeastern University, Shenyang 110819, China*

Complete contact information is available at: https://pubs.acs.org/10.1021/acs.jmedchem.1c00085

Notes

The authors declare no competing financial interest.

■ ACKNOWLEDGMENTS

The authors thank Dr. Dahong Yao from the School of Pharmaceutical Sciences, Shenzhen University, Shenzhen 518000, China, for the molecular docking assay. They are grateful for the financial support from the National Natural Science Foundation of China (no. 32072208).

■ ABBREVIATIONS

BC, breast cancer; DCM, dichloromethane; DMP, Dess−Martin periodinane; DMF, *N*,*N*-dimethylformamide; HPLC, high-performance liquid chromatography; IC_{50}, half-maximal inhibitory concentration; LAH, lithium aluminum hydride; LDA, lithium diisopropylamide; MOMBr, bromomethyl methyl ether; MTT, 3-(4,5-dimethylthiazol-2-yl)-3,5-phenytetrazoliumromide; NMR, nuclear magnetic resonance; PI3K, phosphatidylinositide 3-kinase; PTP1B, protein-tyrosine phosphatase 1B; SARs, structure−activity relationships; TBAF, tetrabutylammonium fluoride; TBSCl, *tert*-butyldimethylsilyl chloride; THF, tetrahydrofuran; TNBC, triple-negative breast cancer

■ REFERENCES

(1) DeSantis, C. E.; Bray, F.; Ferlay, J.; Lortet-Tieulent, J.; Anderson, B. O.; Jemal, A. International variation in female breast cancer incidence and mortality rates. *Cancer Epidemiol., Biomarkers Prev.* **2015**, *24*, 1495−1506.

(2) Sorlie, T.; Perou, C. M.; Tibshirani, R.; Aas, T.; Geisler, S.; Johnsen, H.; Hastie, T.; Eisen, M. B.; van de Rijn, M.; Jeffrey, S. S.; Thorsen, T.; Quist, H.; Matese, J. C.; Brown, P. O.; Botstein, D.; Lonning, P. E.; Borresen-Dale, A. L. Gene expression patterns of breast carcinomas distinguish tumor subclasses with clinical implications. *Proc. Natl. Acad. Sci. U.S.A.* **2001**, *98*, 10869−10874.

(3) Perou, C. M.; Sorlie, T.; Eisen, M. B.; van de Rijn, M.; Jeffrey, S. S.; Rees, C. A.; Pollack, J. R.; Ross, D. T.; Johnsen, H.; Akslen, L. A.; Fluge, O.; Pergamenschikov, A.; Williams, C.; Zhu, S. X.; Lønning, P. E.; Børresen-Dale, A. L.; Brown, P. O.; Botstein, D. Molecular portraits of human breast tumours. *Nature* **2000**, *406*, 747−752.

(4) Polyak, K. Heterogeneity in breast cancer. *J. Clin. Invest.* **2011**, *121*, 3786−3788.

(5) Costa, R. L. B.; Han, H. S.; Gradishar, W. J. Targeting the PI3K/AKT/mTOR pathway in triple-negative breast cancer: a review. *Breast Cancer Res. Treat.* **2018**, *169*, 397−406.

(6) Lehmann, B. D.; Bauer, J. A.; Chen, X.; Sanders, M. E.; Chakravarthy, A. B.; Shyr, Y.; Pietenpol, J. A. Identification of human triple-negative breast cancer subtypes and preclinical models for selection of targeted therapies. *J. Clin. Invest.* **2011**, *121*, 2750−2767.

(7) Anders, C. K.; Carey, L. A. Biology, metastatic patterns, and treatment of patients with triple-negative breast cancer. *Clin. Breast Cancer* **2009**, *9*, S73−S81.

(8) Chavez, K. J.; Garimella, S. V.; Lipkowitz, S. Triple negative breast cancer cell lines: one tool in the search for better treatment of triple negative breast cancer. *Breast Dis.* **2011**, *32*, 35−48.

(9) Wang, W. H.; Xu, H. Y.; Zhao, Z. M.; Zhang, G. M.; Lin, F. W. Dynamic and significant changes of T-cell subgroups in breast cancer patients during surgery and chemotherapy. *Int. Immunopharmacol.* **2018**, *65*, 279−283.

(10) Bianchini, G.; Balko, J. M.; Mayer, I. A.; Sanders, M. E.; Gianni, L. Triple-negative breast cancer: challenges and opportunities of a heterogeneous disease. *Nat. Rev. Clin. Oncol.* **2016**, *13*, 674−690.

(11) Nurgali, K.; Jagoe, R. T.; Abalo, R. Editorial: adverse effects of cancer chemotherapy: anything new to improve tolerance and reduce sequelae? *Front. Pharmacol.* **2018**, *9*, No. 245.

(12) Woods, D.; Turchi, J. J. Chemotherapy induced DNA damage response: convergence of drugs and pathways. *Cancer Biol. Ther.* **2013**, *14*, 379−389.

(13) Teles, R. H. G.; Moralles, H. F.; Cominetti, M. R. Global trends in nanomedicine research on triple negative breast cancer: a bibliometric analysis. *Int. J. Nanomed.* **2018**, *13*, 2321−2336.

(14) Thomsen, A.; Kolesar, J. M. Chemoprevention of breast cancer. *Am. J. Health-Syst. Pharm.* **2008**, *65*, 2221−2228.

(15) Hunter, T. Protein kinases and phosphatases: the yin and yang of protein phosphorylation and signaling. *Cell* **1995**, *80*, 225−236.

(16) Kenner, K. A.; Anyanwu, E.; Olefsky, J. M.; Kusari, J. Protein-tyrosine phosphatase 1B is a negative regulator of insulin- and insulin-like growth factor-I-stimulated signaling. *J. Biol. Chem.* **1996**, *271*, 19810−19816.

(17) Liu, X.; Chen, Q.; Hu, X. G.; Zhang, X. C.; Fu, T. W.; Liu, Q.; Liang, Y.; Zhao, X. L.; Zhang, X.; Ping, Y. F.; Bian, X. W. PTP1B promotes aggressiveness of breast cancer cells by regulating PTEN but not EMT. *Tumour Biol.* **2016**, *37*, 13479−13487.

(18) Li, Y.; Zeng, Q.; Qiu, J.; Pang, T.; Xian, J.; Zhang, X. Long non-coding RNA UCA1 promotes breast cancer by upregulating PTP1B expression via inhibiting miR-206. *Cancer Cell Int.* **2019**, *19*, No. 275.

(19) Yu, M.; Liu, Z.; Liu, Y.; Zhou, X.; Sun, F.; Liu, Y.; Li, L.; Hua, S.; Zhao, Y.; Gao, H.; Zhu, Z.; Na, M.; Zhang, Q.; Yang, R.; Zhang, J.; Yao, Y.; Chen, X. PTP1B markedly promotes breast cancer progression and is regulated by miR-193a-3p. *FEBS J.* **2019**, *286*, 1136−1153.

(20) Hilmarsdottir, B.; Briem, E.; Halldorsson, S.; Kricker, J.; Ingthorsson, S.; Gustafsdottir, S.; Maelandsmo, G. M.; Magnusson, M. K.; Gudjonsson, T. Inhibition of PTP1B disrupts cell-cell adhesion and induces anoikis in breast epithelial cells. *Cell Death Dis.* **2017**, *8*, No. e2769.

(21) Soysal, S.; Obermann, E. C.; Gao, F.; Oertli, D.; Gillanders, W. E.; Viehl, C. T.; Muenst, S. PTP1B expression is an independent positive prognostic factor in human breast cancer. *Breast Cancer Res. Treat.* **2013**, *137*, 637−644.

(22) Wiener, J. R.; Kerns, B. J.; Harvey, E. L.; Conaway, M. R.; Iglehart, J. D.; Berchuck, A.; Bast, R. C., Jr. Overexpression of the protein tyrosine phosphatase PTP1B in human breast cancer: association with p185c-erbB-2 protein expression. *J. Natl. Cancer Inst.* **1994**, *86*, 372−378.

(23) Arias-Romero, L. E.; Saha, S.; Villamar-Cruz, O.; Yip, S. C.; Ethier, S. P.; Zhang, Z. Y.; Chernoff, J. Activation of Src by protein tyrosine phosphatase 1B is required for ErbB2 transformation of human breast epithelial cells. *Cancer Res.* **2009**, *69*, 4582−4588.
(24) Julien, S. G.; Dube, N.; Read, M.; Penney, J.; Paquet, M.; Han, Y.; Kennedy, B. P.; Muller, W. J.; Tremblay, M. L. Protein tyrosine phosphatase 1B deficiency or inhibition delays ErbB2-induced mammary tumorigenesis and protects from lung metastasis. *Nat. Genet.* **2007**, *39*, 338−346.
(25) Lee, S.; Wang, Q. Recent development of small molecular specific inhibitor of protein tyrosine phosphatase 1B. *Med. Res. Rev.* **2007**, *27*, 553−573.
(26) Krishnan, N.; Koveal, D.; Miller, D. H.; Xue, B.; Akshinthala, S. D.; Kragelj, J.; Jensen, M. R.; Gauss, C. M.; Page, R.; Blackledge, M.; Muthuswamy, S. K.; Peti, W.; Tonks, N. K. Targeting the disordered C terminus of PTP1B with an allosteric inhibitor. *Nat. Chem. Biol.* **2014**, *10*, 558−566.
(27) Liu, F.; Yuan, T.; Liu, W.; Ma, H.; Seeram, N. P.; Li, Y.; Xu, L.; Mu, Y.; Huang, X.; Li, L. Phloroglucinol derivatives with protein tyrosine phosphatase 1B inhibitory activities from eugenia *jambolana* seeds. *J. Nat. Prod.* **2017**, *80*, 544−550.
(28) Li, G. Q.; Zhang, Y. B.; Wu, P.; Chen, N. H.; Wu, Z. N.; Yang, L.; Qiu, R. X.; Wang, G. C.; Li, Y. L. New phloroglucinol derivatives from the fruit tree *Syzygium jambos* and their cytotoxic and antioxidant activities. *J. Agric. Food Chem.* **2015**, *63*, 10257−10262.
(29) Yang, J.; Su, J. C.; Lei, X. P.; Huang, X. J.; Zhang, D. M.; Ye, W. C.; Wang, Y. Acylphloroglucinol derivatives from the leaves of *Syzygium samarangense* and their cytotoxic activities. *Fitoterapia* **2018**, *129*, 1−6.
(30) Tringali, C.; Piatelli, M. Two chrome derivatives from the brown alga *Zonaria tournefortii*. *Tetrahedron Lett.* **1982**, *23*, 1509−1512.
(31) Wu, J.; Mu, R.; Sun, M.; Zhao, N.; Pan, M.; Li, H.; Dong, Y.; Sun, Z.; Bai, J.; Hu, M.; Nathan, C. F.; Javid, B.; Liu, G. Derivatives of natural product agrimophol as disruptors of intrabacterial pH homeostasis in mycobacterium tuberculosis. *ACS Infect. Dis.* **2019**, *5*, 1087−1104.
(32) Lawrence, A. L.; Adlington, R. M.; Baldwin, J. E.; Lee, V.; Kershaw, J. A.; Thompson, A. L. A short biomimetic synthesis of the meroterpenoids guajadial and psidial A. *Org. Lett.* **2010**, *12*, 1676−1679.
(33) Li, Y. F.; Yu, B.; Wang, R. X. Efficient synthesis of rottlerin and its two subunits. *Tetrahedron Lett.* **2016**, *57*, 1856−1859.
(34) Elkhalifa, D.; Siddique, A. B.; Qusa, M.; Cyprian, F. S.; El Sayed, K.; Alali, F.; Al Moustafa, A.-E.; Khalil, A. Design, synthesis, and validation of novel nitrogen-based chalcone analogs against triple negative breast cancer. *Eur. J. Med. Chem.* **2020**, *187*, No. 111954.
(35) Huang, K. B.; Wang, F. Y.; Tang, X. M.; Feng, H. W.; Chen, Z. F.; Liu, Y. C.; Liu, Y. N.; Liang, H. Organometallic Gold(III) complexes similar to tetrahydroisoquinoline induce ER-stress-mediated apoptosis and pro-death autophagy in A549 cancer cells. *J. Med. Chem.* **2018**, *61*, 3478−3490.
(36) Kroemer, G.; Galluzzi, L.; Brenner, C. Mitochondrial membrane permeabilization in cell death. *Physiol. Rev.* **2007**, *87*, 99−163.
(37) Marchi, S.; Giorgi, C.; Suski, J. M.; Agnoletto, C.; Bononi, A.; Bonora, M.; De Marchi, E.; Missiroli, S.; Patergnani, S.; Poletti, F.; Rimessi, A.; Duszynski, J.; Wieckowski, M. R.; Pinton, P. Mitochondria-ros crosstalk in the control of cell death and aging. *J. Signal Transduction* **2012**, *2012*, No. 329635.
(38) Ren, B.; Li, D.; Si, L.; Ding, Y.; Han, J.; Chen, X.; Zheng, Q. Alteronol induces cell cycle arrest and apoptosis via increased reactive oxygen species production in human breast cancer T47D cells. *J. Pharm. Pharmacol.* **2018**, *70*, 516−524.
(39) Zhao, M.; Guo, T.; Wang, M.; Zhao, Q.; Liu, Y.; Sun, X.; Wang, H.; Hou, Y. The course of uncarinic acid E-induced apoptosis of HepG2 cells from damage to DNA and p53 activation to mitochondrial release of cytochrome c. *Biol. Pharm. Bull.* **2006**, *29*, 1639−1644.
(40) Chipuk, J. E.; Fisher, J. C.; Dillon, C. P.; Kriwacki, R. W.; Kuwana, T.; Green, D. R. Mechanism of apoptosis induction by inhibition of the anti-apoptotic Bcl-2 proteins. *Proc. Natl. Acad. Sci. U.S.A.* **2008**, *105*, 20327−20332.
(41) Neuzil, J.; Wang, X. F.; Dong, L. F.; Low, P.; Ralph, S. J. Molecular mechanism of 'mitocan'-induced apoptosis in cancer cells epitomizes the multiple roles of reactive oxygen species and Bcl-2 family proteins. *FEBS Lett.* **2006**, *580*, 5125−5129.
(42) Huang, P.; Wang, D.; Su, Y.; Huang, W.; Zhou, Y.; Cui, D.; Zhu, X.; Yan, D. Combination of small molecule prodrug and nanodrug delivery: amphiphilic drug-drug conjugate for cancer therapy. *J. Am. Chem. Soc.* **2014**, *136*, 11748−11756.
(43) Fischer, U.; Jänicke, R. U.; Schulze-Osthoff, K. Many cuts to ruin: a comprehensive update of caspase substrates. *Cell Death Differ.* **2003**, *10*, 76−100.
(44) Perez de Castro, I.; Cárcer, G.; Malumbres, M. A census of mitotic cancer genes: new insights into tumor cell biology and cancer therapy. *Carcinogenesis* **2006**, *28*, 899−912.
(45) Hartwell, L. H.; Kastan, M. B. Cell cycle control and cancer. *Science* **1994**, *266*, 1821−1828.
(46) Wu, C. W.; Storey, K. B. Pattern of cellular quiescence over the hibernation cycle in liver of thirteen-lined ground squirrels. *Cell Cycle* **2012**, *11*, 1714−1726.
(47) Zhang, F.; Taipale, M.; Heiskanen, A.; Laiho, M. Ectopic expression of Cdk6 circumvents transforming growth factor-beta mediated growth inhibition. *Oncogene* **2001**, *20*, 5888−5896.
(48) Akli, S.; Keyomarsi, K. Cyclin E and its low molecular weight forms in human cancer and as targets for cancer therapy. *Cancer Biol. Ther.* **2003**, *2*, 37−46.
(49) Kozar, K.; Ciemerych, M. A.; Rebel, V. I.; Shigematsu, H.; Zagozdzon, A.; Sicinska, E.; Geng, Y.; Yu, Q.; Bhattacharya, S.; Bronson, R. T.; Akashi, K.; Sicinski, P. Mouse development and cell proliferation in the absence of D-cyclins. *Cell* **2004**, *118*, 477−491.
(50) Agami, R.; Bernards, R. Distinct initiation and maintenance mechanisms cooperate to induce G1 cell cycle arrest in response to DNA damage. *Cell* **2000**, *102*, 55−66.
(51) Li, X.; Wang, L.; Shi, D. The design strategy of selective PTP1B inhibitors over TCPTP. *Bioorg. Med. Chem.* **2016**, *24*, 3343−3352.
(52) Han, M. W.; Ryu, I. S.; Lee, J. C.; Kim, S. H.; Chang, H. W.; Lee, Y. S.; Lee, S.; Kim, S. W.; Kim, S. Y. Phosphorylation of PI3K regulatory subunit p85 contributes to resistance against PI3K inhibitors in radioresistant head and neck cancer. *Oral Oncol.* **2018**, *78*, 56−63.
(53) Bollu, L. R.; Mazumdar, A.; Savage, M. I.; Brown, P. H. Molecular pathways: targeting protein tyrosine phosphatases in cancer. *Clin. Cancer Res.* **2017**, *23*, 2136−2142.
(54) Szczepankiewicz, B. G.; Liu, G.; Hajduk, P. J.; Abad-Zapatero, C.; Pei, Z.; Xin, Z.; Lubben, T. H.; Trevillyan, J. M.; Stashko, M. A.; Ballaron, S. J.; Liang, H.; Huang, F.; Hutchins, C. W.; Fesik, S. W.; Jirousek, M. R. Discovery of a potent, selective protein tyrosine phosphatase 1B inhibitor using a linked-fragment strategy. *J. Am. Chem. Soc.* **2003**, *125*, 4087−4096.
(55) Yao, D.; Li, C.; Jiang, J.; Huang, J.; Wang, J.; He, Z.; Zhang, J. Design, synthesis and biological evaluation of novel HDAC inhibitors with improved pharmacokinetic profile in breast cancer. *Eur. J. Med. Chem.* **2020**, *205*, No. 112648.

https://doi.org/10.1021/acs.jmedchem.1c00085
J. Med. Chem. 2021, 64, 6008−6020